Separation and Purification Technology 297 (2022) 121426

Contents lists available at ScienceDirect

Separation and Purification Technology

journal homepage: www.elsevier.com/locate/seppur

One-pot hydrothermal synthesis of magnetic N-doped sludge biochar for efficient removal of tetracycline from various environmental waters

Yongfei Ma [a], Tingmei Lu [a], Jiayi Tang [a], Ping Li [b], Ondřej Mašek [c], Lie Yang [a], Li Wu [a], Liuyang He [a], Yongzhen Ding [d], Feng Gao [b], Xuebin Qi [b,*], Zulin Zhang [a,e,*]

[a] School of Resources and Environmental Engineering, Wuhan University of Technology, Wuhan 430070, China
[b] China-UK Water and Soil Resources Sustainable Utilization Joint Research Centre, Farmland Irrigation Research Institute, Chinese Academy of Agricultural Sciences, Xinxiang 453002, China
[c] UK Biochar Research Centre, School of GeoSciences, University of Edinburgh, Alexander Crum Brown Road, Crew Building, Edinburgh, EH9 3FF, UK
[d] Agro-Environmental Protection Institute, Ministry of Agriculture and Rural Affairs, Tianjin 300191, China
[e] The James Hutton Institute, Craigiebuckler, Aberdeen AB15 8QH, UK

ARTICLE INFO

Keywords:
Sludge
Biochar
Hydrothermal synthesis
Tetracycline
Adsorption mechanisms

ABSTRACT

Efficient removal of zwitterionic tetracycline (TC) from water is a critical environmental challenge which is not fully addressed by conventional treatment technologies. A magnetic N-doped sludge biochar (MNSBC) was the first time synthesized by a simple one-pot hydrothermal method. The maximum adsorption capacity of MNSBC for TC was 197.3 mg/g at 298 K. Solution pH, ionic species/strength and humic acid concentration were the critical factors affecting TC adsorption by MNSBC. Elovich and Freundlich models better describing the experimental data illustrated that TC adsorption onto MNSBC was a multi-layer physicochemical adsorption process. Lewis acid-base, π-π conjugation, electrostatic interactions and pore filling were the main adsorption mechanisms. MNSBC also exhibited excellent adsorption performance for TC in various environmental waters, which achieved removal rates of up to 91.6%, 89.0%, 82.0% and 80.8% in mineral, tap, lake and river waters, respectively. The magnetic susceptibility of MNSBC allowed it to be easily collected after adsorption. Regeneration using NaOH could maintain its sustainable adsorption performance. Furthermore, MNSBC showed a very low release levels of iron and total nitrogen at all pH ranges (from 3 to 11), which suggested its suitability for water treatment applications. This study developed a simple technology for synthesis of effective TC adsorbent for different environmental waters and identified a circular economy pathway to reuse of water industry wastes.

1. Introduction

Various antibiotics including tetracyclines, fluoroquinolones, macrolides, β-lactams, sulfonamides and chloramphenicols had been widely used to prevent and treat diseases [1]. China had overtaken the United States as the world's greatest consumer of antibiotics with annual use of antibiotics exceeding 1.62×10^5 tons. 52% of this amount was used in animal husbandry for improving their growth rate [2]. This led to a discharge of a large amount of unmetabolized antibiotics into the environment via faces and urine which caused serious antibiotics pollution of aquatic ecosystems with potential risks to human health [3]. Tetracycline (TC) was the most widely used veterinary antibiotic, and was one of the most frequently detected antibiotics with the high concentration in natural waters [4]. Efficient removal of TC from water is an urgent problem because removal efficiency of the traditional wastewater treatment technologies is insufficient [5].

Adsorption [6], constructed wetlands [7], advanced oxidation [8] and bioremediation [9] have been studied to eliminate antibiotics from waters. Among these technologies, adsorption had shown numerous benefits, such as cost-effectiveness, simple operation and minimal byproducts generation. The selection of adsorbent was crucial for effective removal of TC. Varieties of adsorbents including biochar [10], carbon nanotubes [11], graphene oxide [12], and clay minerals [13] had been used to adsorb TC. Biochar was mainly produced from biomass wastes (e.g., rice straw and sawdust) [14,15] under oxygen-limited atmosphere, and the superior physicochemical properties guaranteed its promising adsorption capacity for TC. In addition to these biomass resources, there were large amounts of municipal sludge generated at

* Corresponding authors.
E-mail addresses: qxb6301@sina.cn (X. Qi), Zulin.Zhang@hutton.ac.uk (Z. Zhang).

https://doi.org/10.1016/j.seppur.2022.121426
Received 26 April 2022; Received in revised form 1 June 2022; Accepted 2 June 2022
Available online 7 June 2022

wastewater treatment plants (WWTPs) due to rapid population growth and urbanization [16]. The production of municipal sewage sludge in China had reached 6.0×10^7 t in 2020 and kept rising. The cost of sludge management shared about 20–60% of the total running costs of WWTPs [17]. Traditional sludge disposal techniques, such as land filling and incineration might cause groundwater and air pollution, respectively. However, the high organic matter content of municipal sludge enabled it to be an ideal raw material for biochar production [18]. Using sludge biochar (SBC) as the adsorbent to adsorb antibiotics could simultaneously realize resource recovery of byproducts in WWTPs as well as effective removal of antibiotics. Previous studies showed that SBC performed a relatively weak adsorption capacity due to its poor physicochemical characteristics [18,19]. The adsorption capacity of biochar mainly depended on its surface area, pore volume and functional groups [20]. Many technologies (e.g., carbon nanotubes, KOH, $ZnCl_2$ and N-doped modification) have been developed to improve these characteristics of biochar for the better adsorption performance [1,21–23]. The application of carbon nanotubes, KOH, $ZnCl_2$ modifications were limited due to the high cost/toxic impact on organisms, toxic CO generation/high pyrolysis temperature and potential heavy metal release risk, respectively. While N-doping was identified as a promising technique due to the similar size of N and C atoms, which enabled it to easily permeate into the carbon lattice structure of biochar and changed its electron distribution because of the one more outermost electron in N compared to that of C [22]. Also, it could introduce N-containing functional groups which would change biochar structure and surface chemistry [24]. Additionally, the advantages of low cost, no heavy metal/toxic gas release risks enabled it to be a promising technology to modify biochar for its physicochemical properties enhancement. Urea ($CO(NH_2)_2$) was regarded as an ideal N-doping reagent because of its low price and high N content (46.7%), and it had been extensively used to modify biochar for porous composite material production [25]. However, in most cases this approach required impregnation or secondary pyrolysis, which made the process more complex and costly, and achieved only poor activation efficiencies due to the diffusion resistance during impregnation. Hydrothermal process was operated at a closed autoclave using water as the reaction media under moderate temperature (180–280 °C) and self-pressure which was considered as a cost-effective method to enhance the physicochemical properties of biochar [26]. To the best of our knowledge, hydrothermal method has not been used to modify biochar by N-doping. In our previous works, we proved that using $ZnCl_2/FeCl_3$ or KOH combined with $MgCl_2/FeCl_3$ hydrothermal activation could significantly enhance the adsorption performance of SBC [27,28]. In addition to enhance the adsorption performance of biochar by increasing the porous structure of biochar (through hindering the shrinkage of carbon matrix) and Fe-O complexation of $FeCl_3$ modification, it could also introduce magnetic component Fe_3O_4 on biochar surface which provided a workable approach for solid–liquid separation, also this was beneficial for biochar regeneration and reuse in cyclic experiments [29,30]. Herein, $CO(NH_2)_2$ and $FeCl_3$ were the first time used to modify SBC by one-pot hydrothermal activation and used to adsorptive removal of TC from water. To obtain its practical application, TC was added into various types of water to investigate its adsorption performance, and its environmental safety and regeneration were also evaluated in this study.

The main objectives of this study were to: (1) synthesize a $CO(NH_2)_2$ and $FeCl_3$ co-modified SBC (MNSBC) by one-pot hydrothermal method for TC adsorptive removal; (2) investigate the dominant mechanisms of TC adsorption onto MMSBC by model fitting, environmental factors experiments and physicochemical characterization analysis; (3) study the adsorption performance of MNSBC for TC in various actual waters (mineral, tap, lake and river waters); (4) assess the environmental safety (Fe and N dissolution) and sustainable adsorption performance of MNSBC synthesized in this study.

2. Materials and methods

2.1. SBC and MNSBC preparation

All used materials were given in Text S1.

Municipal sludge was dried at 343 K, then it was transported into the tube furnace (BTF1200C, Best Equipment, Hefei, China) for pyrolysis at 673, 773, 873 and 973 K with the heating rate of 10 °C/min under nitrogen atmosphere, and holding time of 120 min. At the end, the produced biochars were cooled to room temperature, and these samples were labeled as SBC-673, SBC-773, SBC-873 and SBC-973, respectively. N-doping was done by adding 5.0 g SBC-873 (the reason for using SBC-873 as the precursor had been confirmed in the section of 3.2 (Fig. 4(a)), and it would be called SBC in the following text) into the solution (60 mL) containing 2.5 g, 5.0 g and 10.0 g $CO(NH_2)_2$, respectively, then they were stirred with a magnetic stirrer at 500 r/min for 60 min. Immediately after that, the mixed solutions were transported into the hydrothermal reactors and underwent continuous hydrothermal activation for 720 min at temperature of 493 K. The activated samples were washed three times with deionized water, then they were dried, grinded and sieved (0.15 mm), and labeled as NSBC-0.5, NSBC-1 and NSBC-2. The preparation of MSBC and MNSBC were using $FeCl_3{\cdot}6H_2O$ (5.0 g) and $FeCl_3{\cdot}6H_2O$ (5.0 g)/$CO(NH_2)_2$ (5.0 g) (the dose of $CO(NH_2)_2$ used here had been confirmed in the section of 3.2) as the modifiers, respectively, and the other operations were the same as those of NSBC-1 (NSBC).

2.2. Batch adsorption experiments

Batch experiments were employed to investigate the adsorption characteristics and mechanisms of TC adsorption onto biochar. Kinetics, isotherms and thermodynamics experiments were conducted to study the adsorption process. Also, the environmental safety as well as regeneration performance of biochar were evaluated in this study. Finally, the TC removal efficiency in various real water samples (mineral, tap, lake and river waters) by MNSBC was investigated. The concentration of TC was measured by ultraviolet spectrophotometry (UV-1500C, Macy China Instruments Inc., Shanghai, China) at the wavelength of 360 nm. All the conditions of experiments were given at the bottom of figures.

Biochar characteristics were provided in Text S2.

3. Results and discussions

3.1. Characterization

The crystal structures of biochars were presented in Fig. 1(a). The characteristic diffraction peaks around $2\theta = 20°$ were identified as the amorphous carbons. The diffraction peaks located at 36.5° (1 1 0), 39.5° (1 0 2), 50.1° (1 1 2), 59.9° (1 2 1) and 68.3° (1 2 2) proved the presence of SiO_2 (JCPDS No.99–0088). The diffraction peaks at $2\theta = 26.3°$ corresponded to the graphite crystals [31]. As expected, the graphitization degree of biochar increased with the pyrolysis temperature, also $FeCl_3$ and $CO(NH_2)_2$ single or co-modification enhanced this characteristic. This was desirable for TC adsorption as π-π conjugation generated between the graphitic structure of biochar and aromatic rings of TC [32]. The diffraction peaks of $2\theta = 30.1°$(2 2 0), 35.4°(3 1 1), 42.9°(4 0 0) and 62.4°(4 4 0) on MSBC and MNSBC were due to the presence of magnetic Fe_3O_4 (JCPDS No.19–0629) [33]. The saturation magnetization value of MNSBC was 9.59 emu/mg (Fig. 1(e)). The great magnetic strength of MNSBC allowed it to be quickly collected after adsorption using a magnet.

The porous structure of biochars before and after modification were determined by BET. The N_2 adsorption/desorption curves of all biochars were typical Ⅳ curves with H_3 hysteresis loops (the slops showed a significant increasing at $P/P_0 = 0.5$–0.8) (Fig. 1(c)), which illustrated mesopores or macropores were generated on biochars [34]. The pore

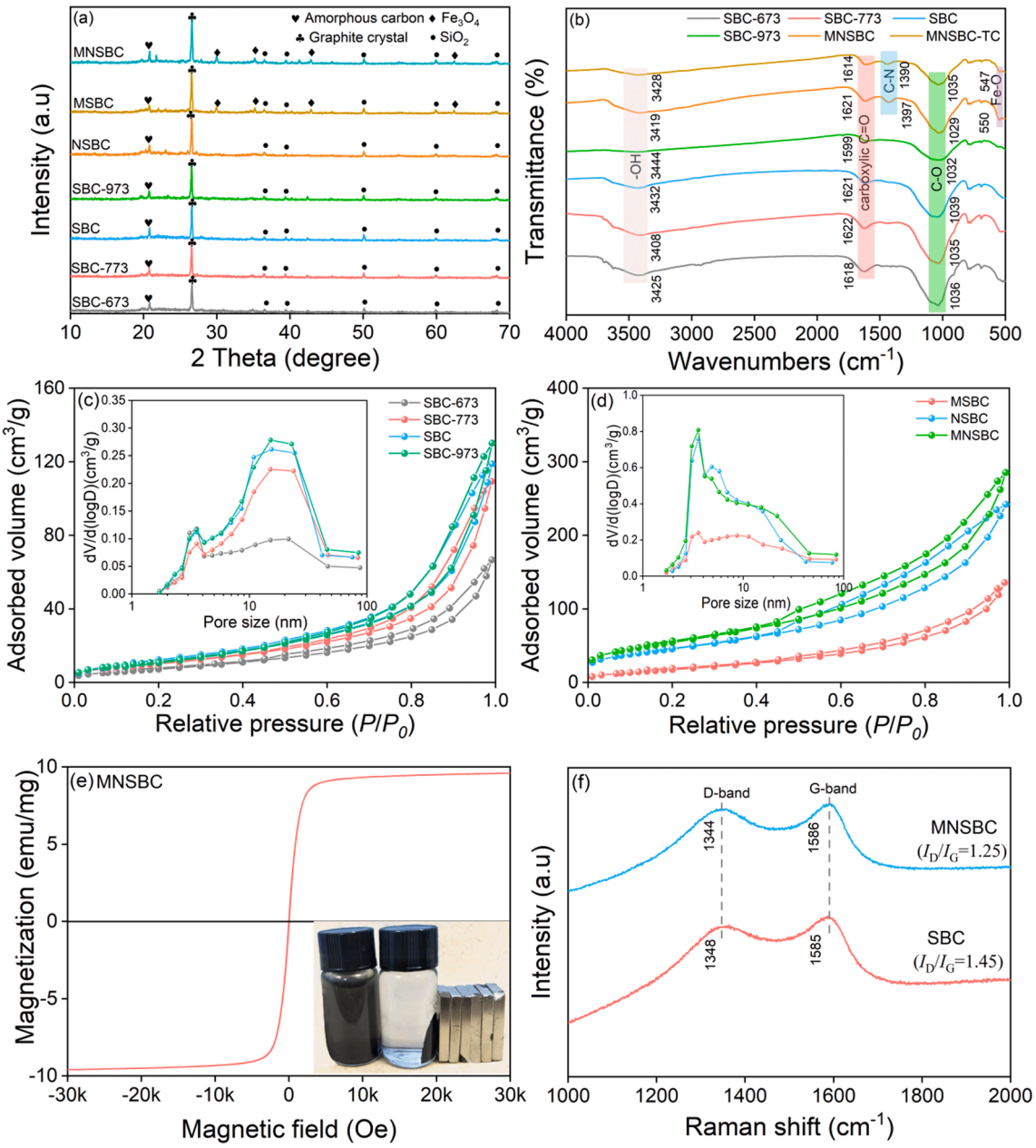

Fig. 1. XRD patterns (a), N_2 adsorption/desorption curves (c) and pore diameter distribution (d) of SBC-673, SBC-773, SBC, SBC-973, MSBC, NSBC and MNSBC; FTIR spectra of SBC-673, SBC-773, SBC, SBC-973, MNSBC and MNSBC-TC (b); magnetic hysteresis loops of MNSBC (e); Raman spectra of SBC and MNSBC (f).

diameter distribution listed in Fig. 1(d) showed that the biochars of SBC-673, SBC-773, SBC and SBC-973 exhibited two pore size characteristics of 3.56 nm and 15.3 nm, and the pore diameter of MSBC, NSBC and MNSBC around 3.64 nm. It was well accepted that the adsorbent would perform the maximal adsorption capacity when the pore diameter of biochar was 1.7–3.0 times that of adsorbate [35]. The pore diameter of MNSBC were mainly concentrated around 3.56 nm, which was 2.89 times of TC molecule size (1.23 × 0.84 × 0.67 nm). This pore size characteristic facilitated the rapid and efficient adsorption of TC by MNSBC. The porous structure parameters listed in Table 1 demonstrated that the S_{BET} and V_{tot} of biochars increased with pyrolysis temperature, and MSBC, NSBC and MNSBC had the larger S_{BET} and V_{tot} (S_{BET} = 113–243 m^2/g and V_{tot} = 0.240–0.469 cm^3/g) than those of SBC (S_{BET} = 44.1–76.5 m^2/g and V_{tot} = 0.115–0.227 cm^3/g). This result illustrated that $FeCl_3$ and $CO(NH_2)_2$ could react with carbon matrix of SBC and increase its porous structure [3].

The surface functional groups on the obtained biochar were presented in Fig. 1(b). The wide bands located at 3408–3444 cm^{-1} were identified as –OH. The characteristic bands at 1599–1622 cm^{-1} and 1029–1039 cm^{-1} corresponded to the presence of carboxylic C = O and C-O, respectively [36,37]. The adsorption peaks of C-N (1397 cm^{-1}) and

Table 1
Pore structure parameters of SBC-673, SBC-773, SBC, SBC-973, MSBC, NSBC and MNSBC.

Biochars	S_{BET} (m^2/g)	V_{tot} (cm^3/g)	D_p (nm)
SBC-673	44.1	0.115	10.4
SBC-773	60.7	0.187	12.3
SBC	72.5	0.205	11.3
SBC-973	76.5	0.227	11.9
MSBC	113	0.240	8.49
NSBC	231	0.420	7.25
MNSBC	243	0.469	7.72

Fe-O (550 cm^{-1}) appeared on MNSBC surface after $FeCl_3$ and $CO(NH_2)_2$ activation, which suggested that N and Fe had embedded into the carbon structure [3]. The band position of Fe-O on MNSBC shifted after TC adsorption, which indicated that it was capable of capturing TC by surface complexation [14]. The –OH on biochar surface was regarded as the predominant functional group because it could bring H-bonding interaction between it (H-donor) and nitrogen, oxygen atoms and aromatic rings of TC (H-acceptors). The position and intensity of –OH on MNSBC changed after TC adsorption which confirmed H-bonding was generated between TC and MNSBC [38]. The stretching vibration intensity of –OH and C = O on MNSBC significantly decreased after TC adsorption, which was assigned to the Lewis acid-base interaction between Lewis acids (–OH and C = O) on MNSBC and Lewis base ($–NH_2$) on TC [39]. Additionally, the stretching vibration intensity of oxygen-containing functional groups (–OH, C = O and C-O) on SBC decreased with increasing pyrolysis temperature.

The Raman spectra of SBC and MNSBC were listed in Fig. 1(f). Two typical characteristic peaks around 1344–1348 cm^{-1} and 1585–1586 cm^{-1} distributed on the Raman spectra of SBC and MNSBC were defined as D-band and G-band, respectively [40]. The stretching vibration of D-band was related to sp^3 hybrid configuration of carbon atom, which reflected the carbon framework defect of biochar. While, G-band described the sp^2 hybridization vibration of graphitic structure. The value of I_D/I_G could be used to evaluate the graphitization degree of biochar [3]. The I_D/I_G values of SBC and MNSBC were 1.45 and 1.25, respectively. Consistent with the above XRD analysis, the lower I_D/I_G value of MNSBC also confirmed that $FeCl_3$ and $CO(NH_2)_2$ co-modification enhanced the graphitization degree of SBC, which facilitated the π-π conjugation between MNSBC and TC.

The SEM-EDS images of SBC and MNSBC were listed in Fig. 2. The results showed that the surface of SBC was smooth, and no obvious pore channels or sheets were observed on its surface (Fig. 2(a)). While, MNSBC exhibited a rough surface with numerous porous and branch structure, and this characteristic improved its porous structure which could provide abundant active sites for TC adsorption (Fig. 2(b)). The results of elemental mapping showed that the main elemental components of SBC and MNSBC were C, O and Si. While the content of Fe and N on MNSBC increased, which suggested that Fe and N were successfully inserted into its carbon skeleton.

XPS spectra was used to investigate the elemental composition and chemical form of biochars. The XPS survey spectra (Fig. 3(a)) showed that SBC and MNSBC had distinct C 1 s (284.8 eV) and O 1 s (532.0 eV) peaks. The new peaks of N 1 s at 400.5 eV and Fe 2p at 712.2 eV in MNSBC spectra clearly illustrated successful embedding of N and Fe in its carbon matrix. The C 1 s of SBC, MNSBC and MNSBC-TC could be divided into three contributions of C-C/C = C (284.8 eV), C-O (285.9, 286.0 and 286.4 eV) and C = O (289.0, 289.1 and 288.5 eV) (Fig. 3(b)). Compared with SBC (C-C/C = C, 68.4%), the greater C-C/C = C content (70.4%) of MNSBC described its greater graphitization degree [32]. This result was consistent with the above XRD and Raman spectra analysis. Additionally, the C-C/C = C ratio of MNSBC reduced after TC adsorption, suggesting its graphitic structure participated in π-π conjugation which facilitated TC adsorption (Fig. 3(b)). The N 1 s of MNSBC was decomposed into four related sub-peaks: pyridinic-N (398.9 eV, 17.0%), pyrrolic-N (400.3 eV, 34.7%), graphitic-N (401.7 eV, 29.5%) and oxidic-N (402.6 eV, 18.8%) [41] (Fig. 3(c)). Compared with MNSBC, the decrease in bonding energy and content of pyridinic-N of MNSBC-TC was due to the Lewis acid-base interaction between pyridinic-N of MNSBC (Lewis base) and –OH of TC (Lewis acid) [22]. In addition, the content and bonding energy of pyrrolic-N on MNSBC surface also decreased. This was assigned to the fact that the introduction of strongly electronegative N atoms reduced the electron density of MNSBC surface [22,42], which enhanced the π-π conjugation interaction between MNSBC (π-electron acceptor) and aromatic rings of TC (π-electron donor) and caused the reduction of pyrrolic-N [43]. The Fe 2p of MNSBC could be decomposed into four peaks of Fe^{2+} $2p_{3/2}$ (711.9 eV), Fe^{3+} $2p_{3/2}$ (714.6 eV), Fe^{2+} $2p_{1/2}$ (725.2.9 eV) and Fe^{3+} $2p_{1/2}$ (728.0 eV) (Fig. 3(d)), which further confirmed that magnetic Fe_3O_4 was successfully loaded on the surface of MNSBC due to the co-existence of Fe^{2+} and Fe^{3+} [44]. The bonding energies of Fe^{2+} $2p_{3/2}$, Fe^{3+} $2p_{3/2}$, Fe^{2+} $2p_{1/2}$ and Fe^{3+} $2p_{1/2}$ of MNSBC decreased after TC adsorption, indicating that complexation interaction was involved between Fe_3O_4 and TC.

3.2. The adsorption capacity of biochars and effect of MNSBC dose on TC removal

Obviously, the adsorption capacity of SBC increased with pyrolysis temperature increasing (Fig. 4(a)) because its greater graphitization degree and superior porous structure prepared at the higher pyrolysis temperature. While no significant difference in the adsorption capacity of SBC and SBC-973, which might be due to the significant decrease in the number of oxygen-containing functional groups on SBC-973 surface.

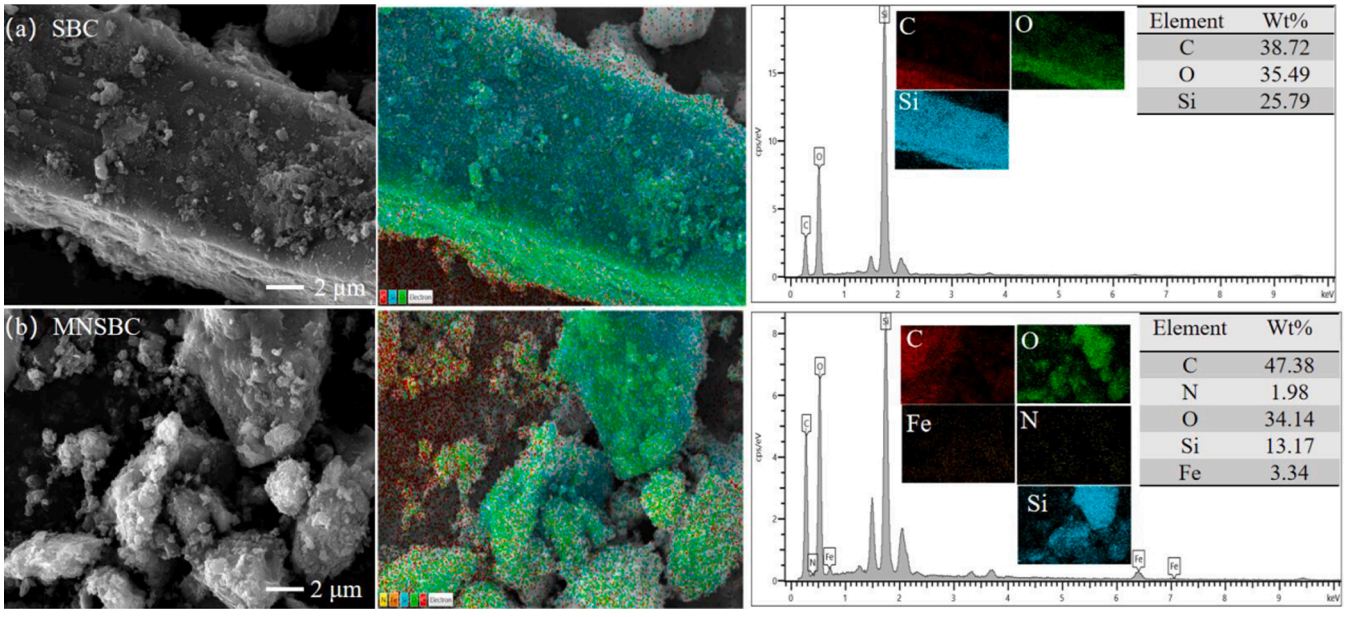

Fig. 2. The SEM-EDS images of SBC (a) and MNSBC (b).

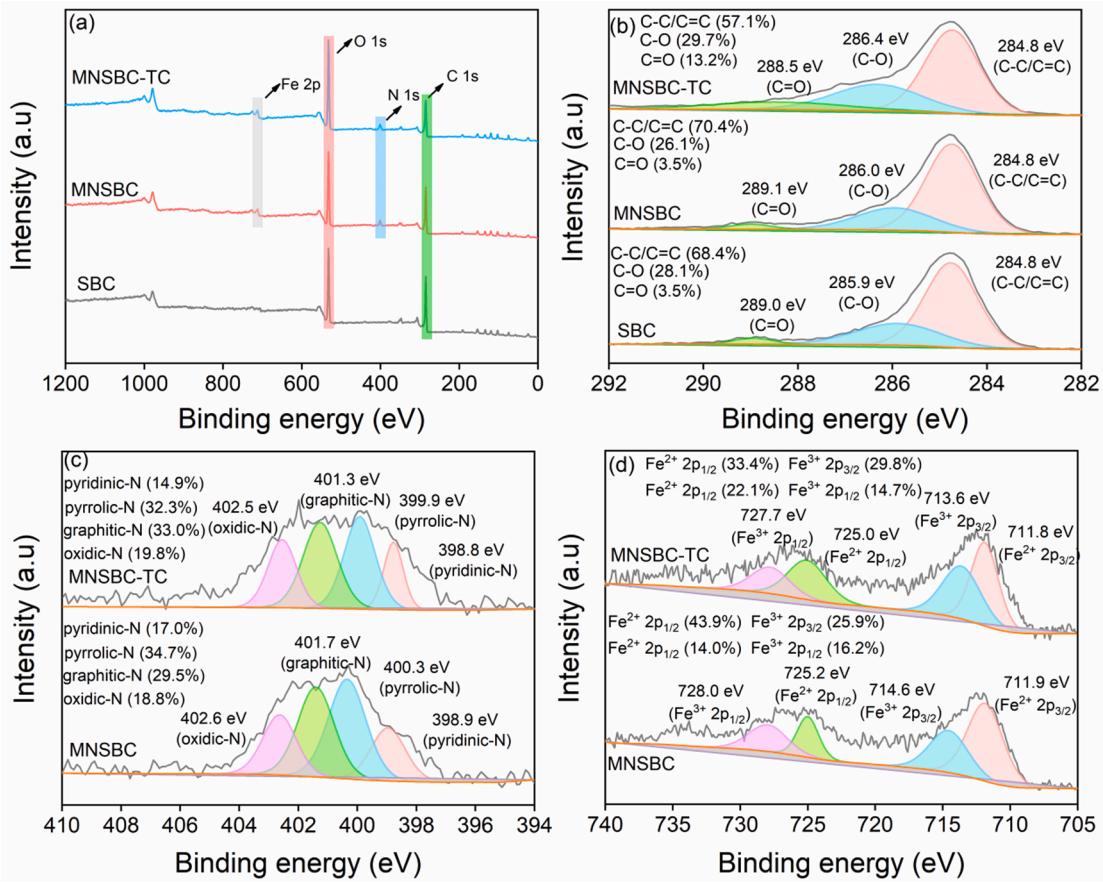

Fig. 3. XPS survey spectra (a); C 1 s of SBC, MNSBC and MNSBC-TC (b); N 1s (c) and Fe 2p (d) of MNSBC and MNSBC-TC.

Fig. S1(a) described that the adsorption capacity of N-doped SBC increased with the mass ratio of $CO(NH_2)_2$/SBC from 0.5:1 to 2:1. While no significant difference in the adsorption capacity of NSBC-1 and NSBC-2 was observed, herein the mass ratio of $CO(NH_2)_2$/SBC = 1:1 was used to modify SBC. Fig. 4 (b) showed the adsorption capacity of SBC, MSBC, NSBC and MNSBC for TC increased with increasing reaction time. MNSBC exhibited a greater adsorption capacity compared to SBC, MSBC and NSBC. The adsorption capacity of MNSBC was 2.18, 1.66 and 1.06 times those of SBC, MSBC and NSBC, respectively. The effect of MNSBC dose in the range of 15–35 mg on TC removal efficiencies was presented in Fig. S1(b). Clearly, the removal efficiencies of TC increased with MNSBC dose because the higher dose could provide more active sites for TC adsorption. The results showed that the removal rates were 70.2%, 80.4%, 92.3%, 94.2% and 95.3% for 15 mg, 10 mg, 25 mg, 30 mg and 35 mg of MNSBC, respectively. Considering the economic cost and high removal efficiency, hence the dose of 25 mg MNSBC was used in the subsequent experiments.

3.3. Adsorption kinetics of SBC and MNSBC

Fig. 4(c and d) showed that the adsorption capacity of biochars depended on the reaction time at the specific TC concentration (C_0 = 20 mg/L). Unsurprisingly, the fastest adsorption occurred at the initial stage, then the adsorption rate dropped dramatically and eventually achieved equilibrium. The initial 240 min was identified as the rapid adsorption process, and about 80.0% and 81.7% of the equilibrium adsorption amount of SBC and MNSBC for TC were accomplished in this stage, respectively. This was due to the weaker diffusion resistance and large numbers of unoccupied active sites. After this stage, the adsorption rate decreased as the concentration of TC decreased and most of the binding sites had been occupied by TC molecules.

Pseudo-first/second-order, and Elovich models (their equations were listed in Text S3) were applied to describe the experimental data of kinetics to study the adsorption mechanisms (Fig. 4 (c)). Pseudo-first-order model assumed that the adsorption rate of biochar was proportional to the ratio of adsorbate concentration/biochar mass [36]. Pseudo-second-order model illustrated that the adsorption process was mainly controlled by the chemical mechanisms including valency forces or electrons exchange [45]. Elovich was another kinetics model used to describe the chemisorption of solid–liquid [34]. The kinetics fitting parameters in Table S1 suggested that Elovich model better describing the adsorption process of TC onto SBC and MNSBC with the greater non-linear correlation coefficient (R^2 = 0.989 and 0.995) than those of pseudo-first-order (R^2 = 0.926 and 0.864) and pseudo-second-order (R^2 = 0.985 and 0.968), also the equilibrium adsorption amount calculated ($q_{e,\ cal}$ (mg/g)) from Elovich agreed better with the experimental value ($q_{e,\ exp}$ (mg/g)). The parameters of a and b in Elovich model were related to the initial adsorption rate constant and desorption rate constant, respectively. The greater ratio value of a/b suggested that the adsorption process of TC onto MNSBC was favorable and irreversible [46], which indicated that a low risk of the adsorbed TC being released into the solution again.

Intraparticle diffusion (its equation was listed in Text S3) was used to investigate the diffusion mechanisms, as well as the dominant rate-limiting step [36]. The fitting plots of q_t against $t^{1/2}$ were divided into two stages, and the first stage was named as liquid-film diffusion and the second one was intraparticle diffusion (Fig. 4(d)). Two plots didn't pass through the origin which suggested that intraparticle diffusion was not the unique rate-limiting step and the whole adsorption process was simultaneously controlled by both liquid-film and intraparticle diffusions. Firstly, TC transported from the bulk solution to the external surface of biochar in the stage of liquid-film diffusion, then the adsorbed

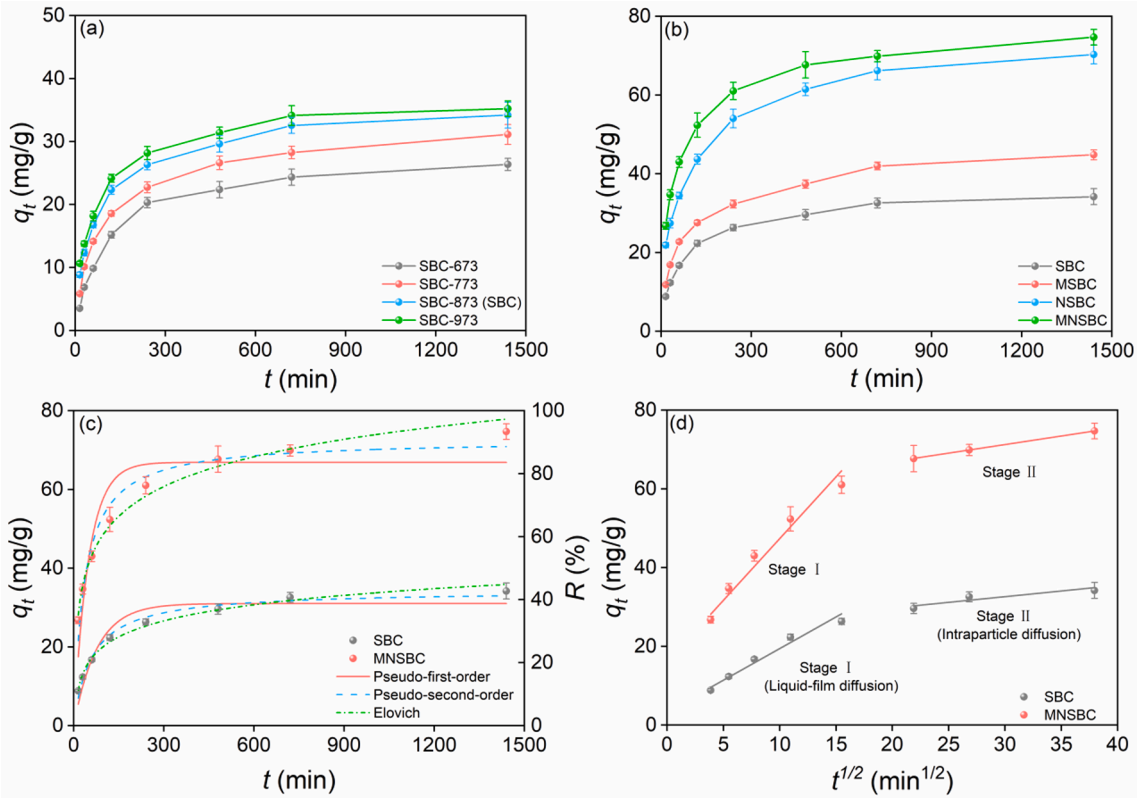

Fig. 4. Effect of pyrolysis temperature on adsorption capacity of SBC for TC (a); adsorption capacity of SBC, MSBC, NSBC and MNSBC for TC (b); kinetics (c) and intraparticle diffusion (d) fitting of TC adsorption onto SBC and MNSBC (C_0 = 20 mg/L, V = 0.1 L, m = 0.025 g, T = 298 K, and t = 0–1440 min).

TC on the outer surface of biochar gradually spread into the inner pores of biochar. The diffusion rate constants of liquid-film diffusion (K_I=1.61 mg/g min$^{1/2}$ and 3.14 mg/g min$^{1/2}$) were greater than those of intraparticle diffusion (K_{II}=0.288 mg/g min$^{1/2}$ and 0.435 mg/g min$^{1/2}$) despite of biochars (Table S2), which illustrated that the step of liquid-film diffusion was more distinct. In addition, the liquid-film diffusion and intraparticle diffusion constants (K_I=3.14 mg/g min$^{1/2}$ and K_{II}=0.435 mg/g min$^{1/2}$) of MNSBC were greater than those of SBC (K_I=1.61 mg/g min$^{1/2}$ and K_{II}=0.288 mg/g min$^{1/2}$) which might be due to its larger S_{BET} and V_{tot} confirmed in BET analysis. >80% of the adsorption capacity was accomplished in the stage of liquid-film diffusion, which suggested that the contribution of TC adsorption through liquid-film diffusion was larger than that of intraparticle diffusion. C was related to the thickness of boundary layer, and C_{II} values were higher than the values of C_I, which demonstrated that the resistance of intraparticle diffusion was greater than that of liquid-film diffusion. This phenomenon was mainly attributed to the larger numbers of unoccupied active sites in the stage of liquid-film diffusion, while most of these active sites had been occupied by TC in the stage of intraparticle diffusion [46].

3.4. Adsorption isotherms

As shown in Fig. 5(a), the equilibrium adsorption amounts of TC on SBC and MNSBC and equilibrium concentrations of TC increased with the initial concentrations of TC (from 20 mg/L to 200 mg/L). Adsorption

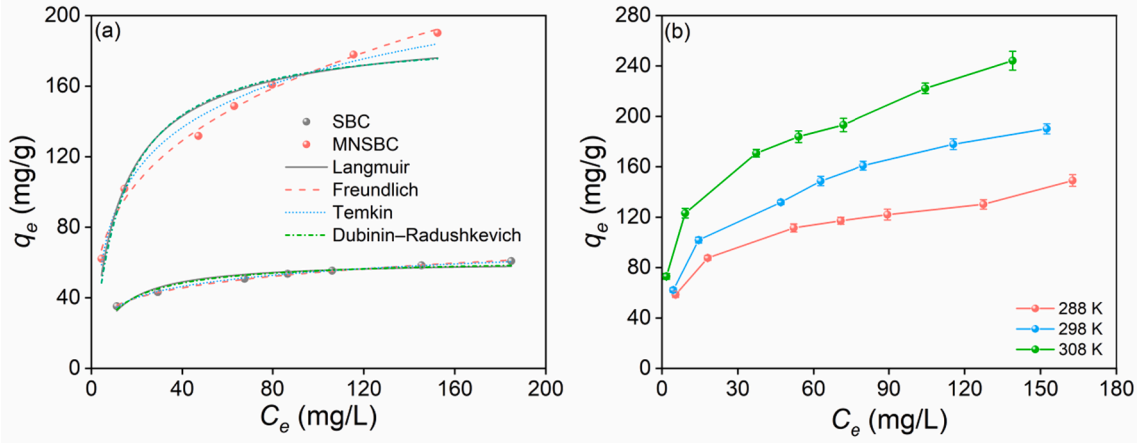

Fig. 5. Isotherms of Langmuir, Freundlich, Temkin and Dubinin–Radushkevich fitting of TC adsorption onto SBC and MNSBC (a); effect of reaction temperature on adsorption capacity of MNSBC for TC (b) (C_0 (TC) = 20–200 mg/L, V = 0.1 L, m = 0.025 g, T = 288–308 K, and t = 1440 min).

isotherms described TC was in dynamic equilibrium between solid and liquid at various concentrations. Four isotherm models including Langmuir, Freundlich, Temkin and Dubinin–Radushkevich (their equations were listed in Text S3) were adopted to fit the experimental data in this study. Langmuir model was proposed based on the hypothesis that the adsorption process was mainly a monolayer chemisorption, and biochar surface was homogeneous. While, Freundlich model assumed that it was a multi-layer physisorption, bonding energy was not equal and the biochar surface was heterogeneous [47]. Generally, Langmuir isotherms model could be applied to estimate the maximal adsorption amounts of biochar. The maximal TC adsorption amounts of MNSBC and SBC calculated by this model were 197.3 mg/g and 63.3 mg/g, respectively. The adsorption capacity of MNSBC (197.3 mg/g) prepared here was significantly larger than those of SBC (63.3 mg/g) (this study), magnetic Auricularia Auricula dregs biochar (42.31 mg/g) [48], alkali modified magnetic rice straw biochar (97.86 mg/g) [14] and spent coffee ground derived biochar (39.22 mg/g) [49]. The fitting results (Fig. 5(a)) and parameters (Table S3) suggested that the isotherms data of SBC and MNSBC agreed better with Freundlich model with the greater non-linear correlation coefficient ($R^2 = 0.998$ and 0.993), also $0 < 1/n < 1$ suggested that this isotherm model was favorable. This result indicated that the adsorption processes of TC onto SBC/MNSBC were multilayer physisorption on their homogeneous surfaces [50]. To further verify the adsorption process of TC onto biochar, Temkin and Dubinin–Radushkevich models were also adopted to fit the experimental data of isotherms. Temkin model described that the adsorption energy was uniformly distributed and it decreased linearly with the surface coverage [51]. It was more suitable for illustrating the chemical adsorption process, and its weaker non-linear correlation coefficients ($R^2 = 0.982$ and 0.984) than those of Freundlich model suggested that chemical interactions were not the only adsorption mechanism. The free energy (E (kJ/mol)$=1/\sqrt{2\beta}$) calculated from Dubinin–Radushkevich model could be used to distinguish the adsorption interactions of physical or chemical [52]. The E values lied between 20 kJ/mol and 40 kJ/mol, which described the chemical interactions were also involved in the adsorption processes of TC adsorption onto SBC and MNSBC.

3.5. Adsorption thermodynamics

Adsorption thermodynamic experiments were conducted to identify the effect of reaction temperature on the adsorption performance of MNSBC for TC. Fig. 5(b) showed that the equilibrium adsorption amounts of MNSBC increased with the initial TC concentration and reaction temperature. This result suggested that the process of TC adsorption onto MNSBC was endothermic. All the parameters calculated by the Gibbs-Helmholtz equations were listed in Table S4. The parameter of $\Delta H > 0$ further confirmed it was an endothermic adsorption process [53]. All the values of ΔG were negative, which illustrated that TC adsorption onto MNSBC was favorable and spontaneous [38]. And, the absolute ΔG value increased with the reaction temperature, which suggested that increasing reaction temperature enhanced the spontaneity of TC adsorption onto MNSBC. In addition, the positive ΔS value demonstrated that the randomness increased on the solid–liquid interface during the process of TC adsorption onto MNSBC.

3.6. Effect of environmental factors

Previous studies described that environmental factor had a significant effect on the adsorption performance of biochar [54,55]. Representative indexes, such as solution pH, ionic species/strength and HA concentration were conducted here to study their effect on TC removal by MNSBC. The electrostatic attraction/repulsion were mainly determined by the ionization species of TC and surface charge of MNSBC. TC was an amphoteric molecule due to its acidic group (phenolic –OH) and basic group (–NH_2). Solution pH was considered as a critical environmental factor controlling the whole adsorption process because it could simultaneously determine the form of TC and zeta potential of MNSBC. Three dissociation constants of TC ($pK_{a1} = 3.3$, $pK_{a2} = 7.7$ and $pK_{a3} = 9.7$) decided its four kinds of existing form at different solution pH. Generally, TC was in form of TC^+ at pH < 3.3, TC^0 at 3.3 < pH < 7.7, TC^- at 7.7 < pH < 9.7, and TC^{2-} at pH > 9.7 (the species distribution calculation of TC was summarized in Text S4) (Fig. 6(a)). Fig. 6(d) described that the zeta potential of MNSBC decreased with pH increasing and the point of zero potential charge (pH_{ZPC}) of MNSBC was 3.45. It was well accepted that the biochar surface was positively charged when the solution pH was below its pH_{ZPC} and bond to the anions, otherwise its surface was negatively charged and bond to the cations. Obviously, MNSBC showed the optimum adsorption performance for TC at pH = 5 because TC was in the form of TC^0, and no electrostatic repulsion was existed between MNSBC and TC. The adsorption capacity of MNSBC was inhibited above or below this pH due to the electrostatic repulsion formation between TC and MNSBC as they were simultaneously positively or negatively charged. Additionally, TC could act as the Lewis acid because of its phenolic –OH, and TC began to deprotonate around pH = 8, and this phenomenon became more apparent when pH > 9.7. OH^- as the Lewis base could easily attract the proton of the phenolic –OH, resulting in the deprotonation of TC and breaking the hydrogen bond between TC and MNSBC [54,55]. Above pH = 9, the intensity of electrostatic repulsion significantly increased because the surface of MNSBC was more negatively charged and TC was mainly in the form of TC^{2-}, and the hydrophobicity of TC significantly reduced, while MNSBC still had considerable adsorption performance for TC because charge assisted hydrogen bond (CAHB) became the main adsorption force and participated in overcoming the increased electrostatic repulsion [56].

To study the effect of ionic species/strength on TC removal by MNSBC, the adsorption capacity of MNSBC was determined in the presence of NaCl, $NaNO_3$, NaH_2PO_4, $NaHCO_3$ and $CaCl_2$. Fig. 6 (f-j) described that the adsorption capacity of MNSBC decreased with the ionic strength increasing despite of the ionic species because these charged ionic compounds could eliminate the repulsive interaction among adsorbents and facilitated them to generate more compact aggregation structure (i.e. squeezing-out effect), which was unfavorable for TC adsorption [55]. However, three inorganic salts of NaCl, $NaNO_3$ and NaH_2PO_4 showed no obvious influence on TC removal by MNSBC, which might be due to the weak squeezing-out effect. To identify the effect of HCO_3^- and $H_2PO_4^-$, the solution pH was adjusted to 9 and 5 (the species distribution calculation of H_2CO_3 and H_3PO_4 were given in Text S4), respectively (Fig. 6 (b and c)). Apparently, the adsorption performance of MNSBC for TC was significantly inhibited in the presence of $NaHCO_3$. This phenomenon was because the hydrolysis of HCO_3^- would cause the alkaline environment and increase the electrostatic repulsion between TC and MNSBC. Also, the existence of $CaCl_2$ significantly inhibited TC removal because Ca^{2+} could bind with the carboxyl on MNSBC surface which disturbed the π-π conjugation between TC and MNSBC [1,57]. Additionally, Ca^{2+} could also bind with TC to form Ca-TC complex, which decreased the affinity of MNSBC for TC [57]. HA was the common organic compound that widely distributed in natural waters [58]. Particularly, the adsorption capacity of MNSBC decreased with the HA concentration increasing because competitive adsorption occurred between TC and HA or generation of HA-TC compound reduced the affinity of MNSBC for TC (Fig. 6(k)).

3.7. Adsorption mechanisms

The mechanisms of TC adsorption onto MNSBC were investigated by characterization, adsorption model fitting and environmental factors experiments analysis. Elovich and Freundlich models better fitted the kinetics and isotherms data, respectively, suggesting that the adsorption process was simultaneously dominated by physicochemical interactions. The well developed graphitic structure of MNSBC could interact with four aromatic rings in the molecular structure of TC through π-π

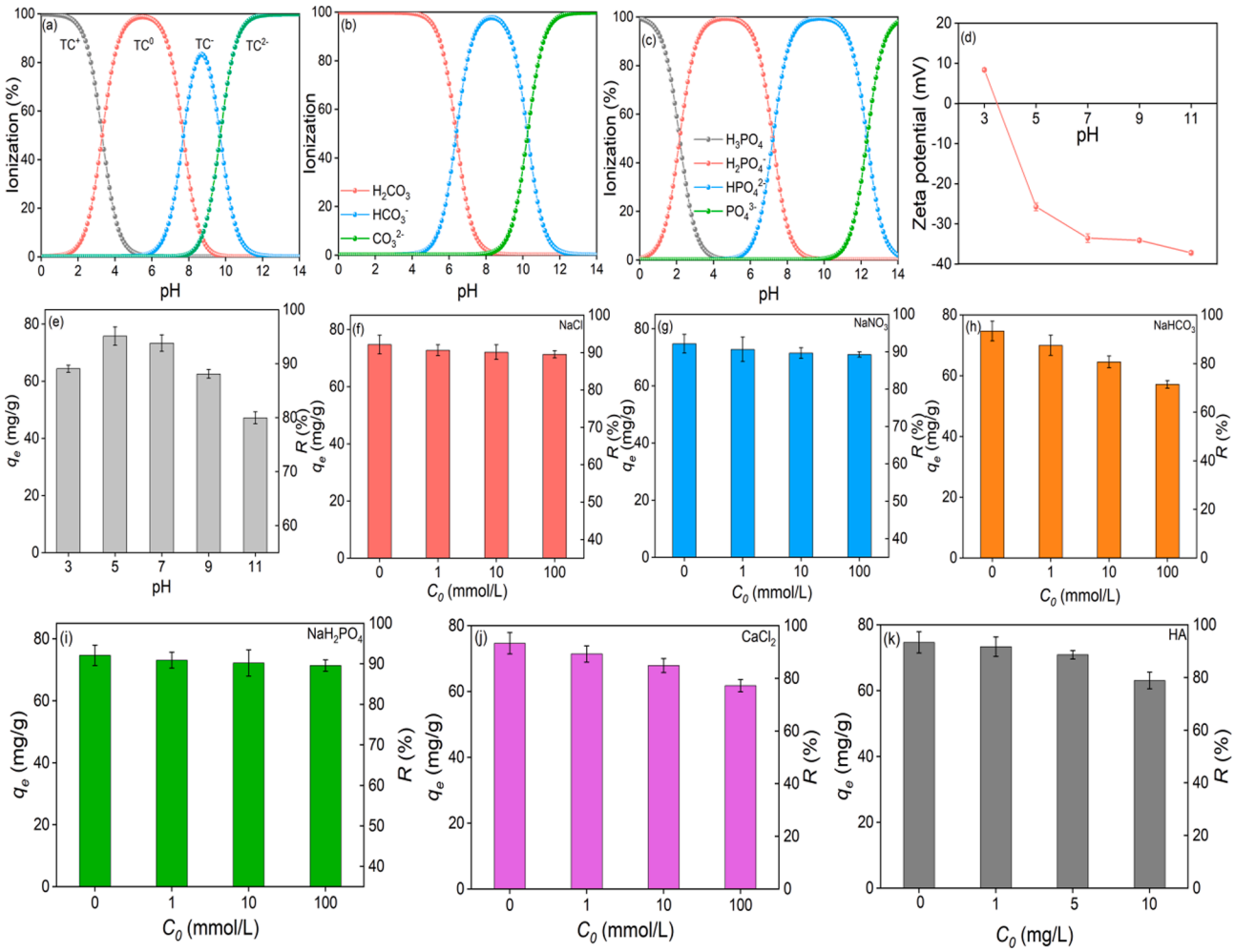

Fig. 6. The species distribution of TC (a), H_2CO_3 (b) and H_3PO_4 (c) at different pH; zeta potential of MNSBC at different pH (from 3 to 11) (d); effect of pH (from 3 to 11) (e), ionic species/strength (NaCl (f), $NaNO_3$ (g), NaH_2PO_4 (pH = 5) (h), $NaHCO_3$ (pH = 9) (i) and $CaCl_2$ (j)) and HA concentration (k) on adsorption performance of MNSBC for TC (C_0 (TC) = 20 mg/L, m = 0.025 g, V = 0.1 L, C_0 (NaCl, $NaNO_3$, NaH_2PO_4, $NaHCO_3$ and $CaCl_2$) = 0–100 mmol/L, C_0 (HA) = 0–10 mg/L).

conjugation (XRD, Raman spectra and XPS analysis). Also, TC could react with MNSBC through cation-π bond between the protonated amino groups and graphite π-electron because its great ionization constant (pK_{a3} value was 9.7) [59]. The C = O, –OH on MNSBC were regarded as the Lewis acids and $–NH_2$ of TC acted as the Lewis base, which caused Lewis acid-base interaction between MNSBC and TC. Additionally, the presence of pyridinic-N on MNSBC (Lewis base) could enhance the Lewis acid-base interaction between MNSBC and phenolic –OH of TC (Lewis acid). The reduction of pyrrolic N on MNSBC after TC adsorption suggested that the introduction of strongly electronegative N atoms reduced the electron density of MNSBC surface, which enhanced the π-π conjugation interaction between MNSBC (π-electron acceptor) and aromatic rings of TC (π-electron donor) (XPS analysis). The adsorption capacity of MNSBC was significantly affected by solution pH and $NaHCO_3$ concentration, indicating that electrostatic interaction could dominate the adsorption process. The inhibitory effect of $CaCl_2$ was mainly attributed to Ca^{2+} which could destroy the π-π conjugation between TC and MNSBC by binding with the carboxyl on MNSBC surface. Also, Ca^{2+} could bind with TC to form Ca-TC complex, which decreased the affinity of MNSBC for TC. The adsorption capacity of MNSBC decreased in the presence of HA, which might be due to the competitive effect of HA or the generation of HA-TC compound reducing the affinity of MNSBC for TC. MNSBC performed the superior porous structure (larger S_{BET} and V_{tot}) than that of SBC, which provided abundant binding sites for TC adsorption by pore filling (SEM and BET analysis). The decrease in bonding energy of Fe 2p (Fe^{2+} $2p_{3/2}$, Fe^{3+} $2p_{3/2}$, Fe^{2+} $2p_{1/2}$ and Fe^{3+} $2p_{1/2}$) (XPS analysis) and change of Fe-O band (FTIR analysis) on MNSBC after TC adsorption illustrated that Fe_3O_4 could adsorb TC though surface complexation. The thermodynamic parameters suggested that the process of TC adsorption onto MNSBC was spontaneous, endothermic and randomness increasing.

3.8. The adsorption performance of MNSBC for TC in various real waters

Various real water samples, including deionized, mineral, tap, lake and river waters (the basic physicochemical properties of these waters were listed in Table S5) were conducted in this study to further verify the adsorption performance of MNSBC for TC. The water samples of tap water and mineral water were obtained from Wuhan University of Technology and Wuhan Mingxinquan Pure Water Co., Ltd., respectively. Lake water and river water were collected at south lake of Wuhan (30°50′ N, 114°35′ E) and Wuhan section of Yangtze River (30°10′ N, 114°09′ E), respectively. Considering that the real environmental waters might affect the results measured by ultraviolet spectrophotometry, the residual concentrations of TC in these real waters were determined by high performance liquid chromatography (HPLC, 1260 Infinity, Agilent Technologies) equipped with a ZORBAX SB-C18 column (5 μm, 4.6 × 150 mm, Agilent) at the determination wavelength of 360 nm. The mobile phase was a mixture of 0.1% formic acid and methanol (V/V = 75/25) with a flow rate of 0.8 mL/min. Fig. 7(a) showed that MNSBC had excellent TC adsorption performance in deionized water (93.4%),

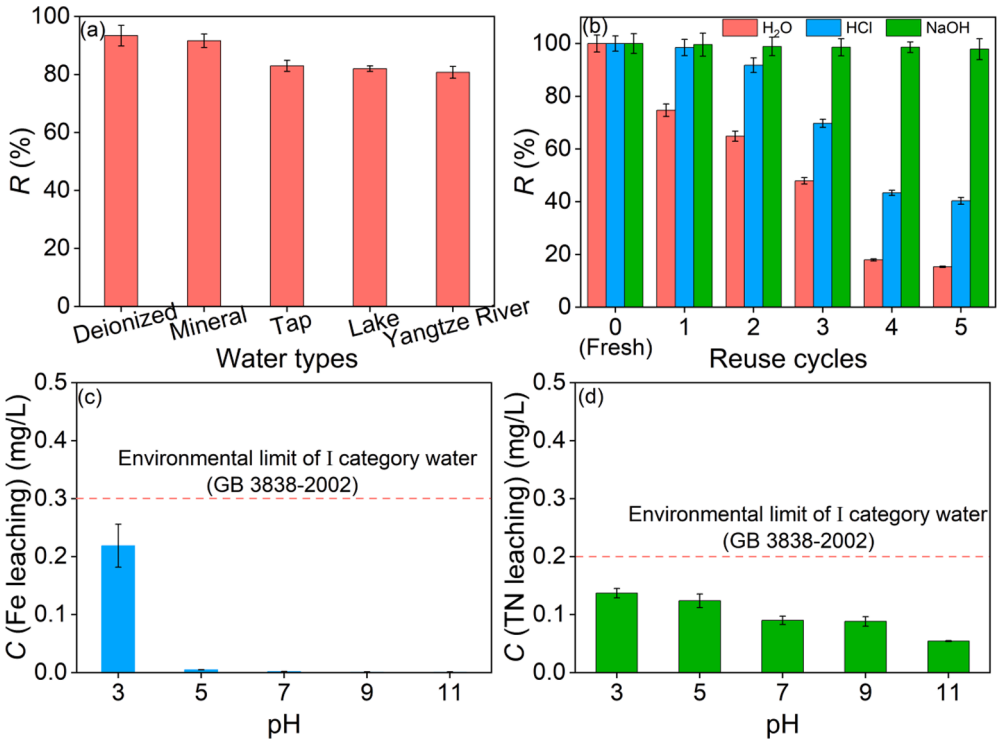

Fig. 7. The removal efficiency of MNSBC for TC in various real waters (a); regeneration of MNSBC in reuse cycles by H_2O, HCl and NaOH treatment (b); effect of solution pH on Fe (c) and TN (d) leaching levels of MNSBC (pH = 3–11) (C_0 (TC) = 20 mg/L, m = 0.025 g, V = 0.1 L, T = 298 K, and t = 1440 min).

mineral water (91.6%), tap water (89.0%), lake water (82.1%), and river water (80.8%). The removal efficiency of TC in lake water and river water by MNSBC were slightly inhibited, which might be related to the inorganic compounds (e.g., N and P) had occupied some active sites of MNSBC because the concentrations of TN (reduced by 73.6% and 66.7%, respectively) and TP (reduced by 71.7% and 71.1%, respectively) were significantly decreased after adsorption.

3.9. The regeneration and environmental safety of MNSBC

The possibility to regenerate biochar after TC adsorption is a critical indicator to determine economic feasibility of its use [60]. Two inorganic solvents, namely HCl (0.1 mol/L) and NaOH (0.1 mol/L) were used to regenerate MNSBC in this study because the solubility of TC would increase in the acidic or alkaline condition which facilitated the adsorbed TC to release into the solution, and H_2O treatment as control. Also, the protonation state of the surface functional groups would change when using acid or alkali to regenerate adsorbent, breaking the adsorption equilibrium and resulting in the desorption of the adsorbate from the adsorbent [1]. The results presented in Fig. 7(b) demonstrated that the adsorption capacity of the used MNSBC decreased using H_2O and HCl regeneration in the reuse cycles. After five reuse cycles, the adsorption capacity of MNSBC were 15.3% and 40.3% of its initial performance by H_2O and HCl treatment, respectively. While, MNSBC maintained a high TC adsorption capacity (97.9% of the initial adsorption capacity) even after five cycles of reuse using NaOH regeneration, which suggested that MNSBC was a promising adsorbent with excellent sustainable adsorption performance by NaOH regeneration.

As leaching of N into water bodies could result in eutrophication, and release of Fe might cause secondary water pollution, the extent to which N and Fe was released by the MNSBC in different pH environments was assessed. Results in Fig. 7(c and d) showed that the leaching levels of Fe and TN were below the national (China) environmental limit values of GB 3838–2002 (C(Fe) = 0.3 mg/L and C(TN) = 0.2 mg/L (I category water)) at all pH levels tested in this study. This result suggested that MNSBC could be applied safely in water treatment, at least from the perspective of Fe and N release.

4. Conclusions

This study successfully synthesized the MNSBC, which showed excellent adsorption capacity for TC as a result of its superior physicochemical characteristics (e.g., larger S_{BET}, V_{tot}, greater graphitization degree and N-doping). Lewis acid-base, π-π conjugation, electrostatic interactions and pore filling were identified as the main adsorption mechanisms. The added N and Fe were safely embedded in the carbon matrix of the MNSBC, as demonstrated by leaching tests at different pH levels (from 3 to 11). Furthermore, MNSBC showed a sustained adsorption capacity even after multiple cycles of regeneration using NaOH, maintaining over 97% of its capacity after five cycles. The excellent TC adsorption performance of MNSBC was demonstrated not only in simulated water samples using deionized water, but also real water samples using mineral water, tap water, lake water and river water, indicating a true potential for real world application. This study identified a promising approach for municipal sludge resource utilization in water treatment for removal of TC, and potentially other applications.

CRediT authorship contribution statement

Yongfei Ma: Conceptualization, Data curation, Visualization, Writing – original draft. **Tingmei Lu:** Data curation, Visualization, Formal analysis. **Jiayi Tang:** Data curation, Visualization, Formal analysis. **Ping Li:** Formal analysis, Writing – review & editing. **Ondřej Mašek:** Formal analysis, Writing – review & editing. **Lie Yang:** Writing – review & editing, Resources, Funding acquisition. **Li Wu:** Methodology, Project administration, Investigation. **Liuyang He:** Data curation, Validation. **Yongzhen Ding:** Writing – review & editing, Supervision. **Feng Gao:** Writing – review & editing, Methodology. **Xuebin Qi:** Writing – review & editing. **Zulin Zhang:** Conceptualization, Writing –

review & editing, Resources, Funding acquisition.

Declaration of Competing Interest

The authors declare that they have no known competing financial interests or personal relationships that could have appeared to influence the work reported in this paper.

Acknowledgements

This work was supported by the National Natural Science Foundation of China (No. 52170171, and No.51878523), Central Public-interest Scientific Institution Basal Research Fund (No. Y2022GH10), the "111" Project of China and the Scottish Government's Rural and Environment Science and Analytical Service Division (RESAS).

Appendix A. Supplementary material

Supplementary data to this article can be found online at https://doi.org/10.1016/j.seppur.2022.121426.

References

[1] L. Yan, Y. Liu, Y. Zhang, S. Liu, C. Wang, W. Chen, C. Liu, Z. Chen, Y. Zhang, $ZnCl_2$ modified biochar derived from aerobic granular sludge for developed microporosity and enhanced adsorption to tetracycline, Bioresour. Technol. 297 (2020), 122381.
[2] Q. Zhang, G. Ying, C. Pan, Y. Liu, J. Zhao, Comprehensive Evaluation of Antibiotics Emission and Fate in the River Basins of China: Source Analysis, Multimedia Modeling, and Linkage to Bacterial Resistance, Environ. Sci. Technol. 49 (2015) 6772–6782.
[3] Y. Mei, J. Xu, Y. Zhang, B. Li, S. Fan, H. Xu, Effect of Fe–N modification on the properties of biochars and their adsorption behavior on tetracycline removal from aqueous solution, Bioresour. Technol. 325 (2021), 124732.
[4] R. Daghrir, P. Drogui, Tetracycline antibiotics in the environment: a review, Environ. Chem. Lett. 11 (2013) 209–227.
[5] G. Chen, S. He, G. Shi, Y. Ma, C. Ruan, X. Jin, Q. Chen, X. Liu, H. Dai, X. Chen, D. Huang, In-situ immobilization of ZIF-67 on wood aerogel for effective removal of tetracycline from water, Chem. Eng. J. 423 (2021), 130184.
[6] G. Wu, J. Ma, S. Li, J. Guan, B. Jiang, L. Wang, J. Li, X. Wang, L. Chen, Magnetic copper-based metal organic framework as an effective and recyclable adsorbent for removal of two fluoroquinolone antibiotics from aqueous solutions, J. Colloid Interf. Sci. 528 (2018) 360–371.
[7] X. Li, W. Zhu, G. Meng, C. Zhang, R. Guo, Efficiency and kinetics of conventional pollutants and tetracyclines removal in integrated vertical-flow constructed wetlands enhanced by aeration, J. Environ. Manage. 273 (2020), 111120.
[8] Q. Zhong, Q. Lin, W. He, H. Fu, Z. Huang, Y. Wang, L. Wu, Study on the nonradical pathways of nitrogen-doped biochar activating persulfate for tetracycline degradation, Sep. Purif. Technol. 276 (2021), 119354.
[9] L. Leng, L. Wei, Q. Xiong, S. Xu, W. Li, S. Lv, Q. Lu, L. Wan, Z. Wen, W. Zhou, Use of microalgae based technology for the removal of antibiotics from wastewater: A review, Chemosphere 238 (2020) 124680.
[10] H.M. Jang, E. Kan, Engineered biochar from agricultural waste for removal of tetracycline in water, Bioresour. Technol. 284 (2019) 437–447.
[11] L. Yi, L. Zuo, C. Wei, H. Fu, X. Qu, S. Zheng, Z. Xu, Y. Guo, H. Li, D. Zhu, Enhanced adsorption of bisphenol A, tylosin, and tetracycline from aqueous solution to nitrogen-doped multiwall carbon nanotubes via cation-π and π-π electron-donor-acceptor (EDA) interactions, Sci. Total Environ. 719 (2020), 137389.
[12] Z.A. ALOthman, N. AlMasoud, X.Y. Mbianda, I. Ali, Synthesis and characterization of γ-cyclodextrin-graphene oxide nanocomposite: Sorption, kinetics, thermodynamics and simulation studies of tetracycline and chlortetracycline antibiotics removal in water, J. Mol. Liq. 345 (2022) 116993.
[13] M. Wu, S. Zhao, R. Jing, Y. Shao, X. Liu, F. Lv, X. Hu, Q. Zhang, Z. Meng, A. Liu, Competitive adsorption of antibiotic tetracycline and ciprofloxacin on montmorillonite, Appl. Clay Sci. 180 (2019), 105175.
[14] J. Dai, X. Meng, Y. Zhang, Y. Huang, Effects of modification and magnetization of rice straw derived biochar on adsorption of tetracycline from water, Bioresour. Technol. 311 (2020), 123455.
[15] X. Zhang, Y. Li, M. Wu, Y. Pang, Z. Hao, M. Hu, R. Qiu, Z. Chen, Enhanced adsorption of tetracycline by an iron and manganese oxides loaded biochar: Kinetics, mechanism and column adsorption, Bioresour. Technol. 320 (2021), 124264.
[16] G. Kor-Bicakci, C. Eskicioglu, Recent developments on thermal municipal sludge pretreatment technologies for enhanced anaerobic digestion, Renew. Sust. Energ. Rev. 110 (2019) 423–443.
[17] A. Gopinath, G. Divyapriya, V. Srivastava, A.R. Laiju, P.V. Nidheesh, M.S. Kumar, Conversion of sewage sludge into biochar: A potential resource in water and wastewater treatment, Environ. Res. 194 (2021), 110656.
[18] H. Liu, G. Xu, G. Li, Preparation of porous biochar based on pharmaceutical sludge activated by NaOH and its application in the adsorption of tetracycline, J. Colloid Interf. Sci. 587 (2021) 271–278.
[19] Y. Ma, P. Li, L. Yang, L. Wu, L. He, F. Gao, X. Qi, Z. Zhang, Iron/zinc and phosphoric acid modified sludge biochar as an efficient adsorbent for fluoroquinolones antibiotics removal, Ecotox. Environ. Safe. 196 (2020), 110550.
[20] O. Paunovic, S. Pap, S. Maletic, M.A. Taggart, N. Boskovic, M., Turk Sekulic, Ionisable emerging pharmaceutical adsorption onto microwave functionalised biochar derived from novel lignocellulosic waste biomass, J. Colloid Interf. Sci. 547 (2019) 350–360.
[21] Y. Wu, H. Cheng, D. Pan, L. Zhang, W. Li, Y. Song, Y. Bian, X. Jiang, J. Han, Potassium hydroxide-modified algae-based biochar for the removal of sulfamethoxazole: Sorption performance and mechanisms, J. Environ. Manage. 293 (2021), 112912.
[22] L. Wang, W. Yan, C. He, H. Wen, Z. Cai, Z. Wang, Z. Chen, W. Liu, Microwave-assisted preparation of nitrogen-doped biochars by ammonium acetate activation for adsorption of acid red 18, Appl. Surf. Sci. 433 (2018) 222–231.
[23] Y. Ma, L. Yang, L. Wu, P. Li, X. Qi, L. He, S. Cui, Y. Ding, Z. Zhang, Carbon nanotube supported sludge biochar as an efficient adsorbent for low concentrations of sulfamethoxazole removal, Sci. Total Environ. 718 (2020), 137299.
[24] L. Leng, S. Xu, R. Liu, T. Yu, X. Zhuo, S. Leng, Q. Xiong, H. Huang, Nitrogen containing functional groups of biochar: An overview, Bioresour. Technol. 298 (2020) 122286.
[25] X. Pei, X. Peng, X. Jia, P.K. Wong, N-doped biochar from sewage sludge for catalytic peroxydisulfate activation toward sulfadiazine: Efficiency, mechanism, and stability, J. Hazard. Mater. 419 (2021) 126446.
[26] T.-B. Nguyen, Q.-M. Truong, C.-W. Chen, R.-a. Doong, W.-H. Chen, C.-D. Dong, Mesoporous and adsorption behavior of algal biochar prepared via sequential hydrothermal carbonization and $ZnCl_2$ activation, Bioresour. Technol. 346 (2022) 126351.
[27] Y. Ma, M. Li, P. Li, L. Yang, L. Wu, F. Gao, X. Qi, Z. Zhang, Hydrothermal synthesis of magnetic sludge biochar for tetracycline and ciprofloxacin adsorptive removal, Bioresour. Technol. 319 (2021), 124199.
[28] Y. Ma, T. Lu, L. Yang, L. Wu, P. Li, J. Tang, Y. Chen, F. Gao, S. Cui, X. Qi, Z. Zhang, Efficient adsorptive removal of fluoroquinolone antibiotics from water by alkali and bimetallic salts co-hydrothermally modified sludge biochar, Environ. Pollut. 298 (2022), 118833.
[29] W. Cai, J. Wei, Z. Li, Y. Liu, J. Zhou, B. Han, Preparation of amino-functionalized magnetic biochar with excellent adsorption performance for Cr(VI) by a mild one-step hydrothermal method from peanut hull, Colloids Surf. A. 563 (2019) 102–111.
[30] W. Zhao, Y. Tian, X. Chu, L. Cui, H. Zhang, M. Li, P. Zhao, Preparation and characteristics of a magnetic carbon nanotube adsorbent: Its efficient adsorption and recoverable performances, Sep. Purif. Technol. 257 (2021), 117917.
[31] J. Wei, Y. Liu, J. Li, Y. Zhu, H. Yu, Y. Peng, Adsorption and co-adsorption of tetracycline and doxycycline by one-step synthesized iron loaded sludge biochar, Chemosphere 236 (2019), 124254.
[32] S. Ho, Y. Chen, R. Li, C. Zhang, Y. Ge, G. Cao, M. Ma, X. Duan, S. Wang, N. Ren, N-doped graphitic biochars from C-phycocyanin extracted Spirulina residue for catalytic persulfate activation toward nonradical disinfection and organic oxidation, Water Res. 159 (2019) 77–86.
[33] W. Lu, J. Li, Y. Sheng, X. Zhang, J. You, L. Chen, One-pot synthesis of magnetic iron oxide nanoparticle-multiwalled carbon nanotube composites for enhanced removal of Cr(VI) from aqueous solution, J. Colloid Interf. Sci. 505 (2017) 1134–1146.
[34] S. Álvarez-Torrellas, M. Muñoz, J.A. Zazo, J.A. Casas, J. García, Synthesis of high surface area carbon adsorbents prepared from pine sawdust- Onopordum acanthium L. for nonsteroidal anti-inflammatory drugs adsorption, J. Environ. Manage. 183 (2016) 294–305.
[35] L. Tang, J. Yu, Y. Pang, G. Zeng, Y. Deng, J. Wang, X. Ren, S. Ye, B. Peng, H. Feng, Sustainable efficient adsorbent: Alkali-acid modified magnetic biochar derived from sewage sludge for aqueous organic contaminant removal, Chem. Eng. J. 336 (2018) 160–169.
[36] X. Geng, S. Lv, J. Yang, S. Cui, Z. Zhao, Carboxyl-functionalized biochar derived from walnut shells with enhanced aqueous adsorption of sulfonamide antibiotics, J. Environ. Manage. 280 (2021), 111749.
[37] X. Feng, B. Qiu, D. Sun, Enhanced naproxen adsorption by a novel β-cyclodextrin immobilized the three-dimensional macrostructure of reduced graphene oxide and multiwall carbon nanotubes, Sep. Purif. Technol. 290 (2022), 120837.
[38] T. Atugoda, C. Gunawardane, M. Ahmad, M. Vithanage, Mechanistic interaction of ciprofloxacin on zeolite modified seaweed (Sargassum crassifolium) derived biochar: Kinetics, isotherm and thermodynamics, Chemosphere 281 (2021), 130676.
[39] H. Zhao, X. Liu, Z. Cao, Y. Zhan, X. Shi, Y. Yang, J. Zhou, J. Xu, Adsorption behavior and mechanism of chloramphenicols, sulfonamides, and non-antibiotic pharmaceuticals on multi-walled carbon nanotubes, J. Hazard. Mater. 310 (2016) 235–245.
[40] W. Shi, H. Wang, J. Yan, L. Shan, G. Quan, X. Pan, L. Cui, Wheat straw derived biochar with hierarchically porous structure for bisphenol A removal: Preparation, characterization, and adsorption properties, Sep. Purif. Technol. 289 (2022), 120796.
[41] K. Zhong, M. Li, Y. Yang, H. Zhang, B. Zhang, J. Tang, J. Yan, M. Su, Z. Yang, Nitrogen-doped biochar derived from watermelon rind as oxygen reduction catalyst in air cathode microbial fuel cells, Appl. Energ. 242 (2019) 516–525.
[42] L. Wang, D. Zhu, L. Duan, W. Chen, Adsorption of single-ringed N- and S-heterocyclic aromatics on carbon nanotubes, Carbon 48 (13) (2010) 3906–3915.

[43] F. Lian, G. Cui, Z. Liu, L. Duo, G. Zhang, B. Xing, One-step synthesis of a novel N-doped microporous biochar derived from crop straws with high dye adsorption capacity, J. Environ. Manage. 176 (2016) 61–68.
[44] M. Jia, Z. Yang, W. Xiong, J. Cao, Y. Xiang, H. Peng, Y. Jing, C. Zhang, H. Xu, P. Song, Magnetic heterojunction of oxygen-deficient Ti3+-TiO2 and Ar-Fe2O3 derived from metal-organic frameworks for efficient peroxydisulfate (PDS) photo-activation, Appl. Catal. B. 298 (2021), 120513.
[45] X. Liu, Y. Guo, C. Zhang, X. Huang, K. Ma, Y. Zhang, Preparation of graphene oxide/4A molecular sieve composite and evaluation of adsorption performance for Rhodamine B, Sep. Purif. Technol. 286 (2022), 120400.
[46] K.C. Bedin, A.C. Martins, A.L. Cazetta, O. Pezoti, V.C. Almeida, KOH-activated carbon prepared from sucrose spherical carbon: Adsorption equilibrium, kinetic and thermodynamic studies for Methylene Blue removal, Chem. Eng. J. 286 (2016) 476–484.
[47] C. Hu, J. Jiang, Y. Li, Y. Wu, J. Ma, H. Li, H. Zheng, Eco-friendly poly(dopamine)-modified glass microspheres as a novel self-floating adsorbent for enhanced adsorption of tetracycline, Sep. Purif. Technol. 292 (2022), 121046.
[48] F. Gao, Z. Xu, Y. Dai, Removal of tetracycline from wastewater using magnetic biochar: A comparative study of performance based on the preparation method, Environ. Technol. Inno. 24 (2021), 101916.
[49] V. Nguyen, T. Nguyen, C. Chen, C. Hung, T. Vo, J. Chang, C. Dong, Influence of pyrolysis temperature on polycyclic aromatic hydrocarbons production and tetracycline adsorption behavior of biochar derived from spent coffee ground, Bioresour. Technol. 284 (2019) 197–203.
[50] A.R. Bagheri, M. Arabi, M. Ghaedi, A. Ostovan, X. Wang, J. Li, L. Chen, Dummy molecularly imprinted polymers based on a green synthesis strategy for magnetic solid-phase extraction of acrylamide in food samples, Talanta 195 (2019) 390–400.
[51] Y. Sun, H. Li, G. Li, B. Gao, Q. Yue, X. Li, Characterization and ciprofloxacin adsorption properties of activated carbons prepared from biomass wastes by H_3PO_4 activation, Bioresour. Technol. 217 (2016) 239–244.
[52] Y. Zhou, X. Liu, Y. Xiang, P. Wang, J. Zhang, F. Zhang, J. Wei, L. Luo, M. Lei, L. Tang, Modification of biochar derived from sawdust and its application in removal of tetracycline and copper from aqueous solution: Adsorption mechanism and modelling, Bioresour. Technol. 245 (2017) 266–273.
[53] W. Deng, D. Zhang, X. Zheng, X. Ye, X. Niu, Z. Lin, M. Fu, S. Zhou, Adsorption recovery of phosphate from waste streams by Ca/Mg-biochar synthesis from marble waste, calcium-rich sepiolite and bagasse, J. Clean. Prod. 288 (2021), 125638.
[54] Q. Duan, X. Li, Z. Wu, A. Alsaedi, T. Hayat, C. Chen, J. Li, Adsorption of 17β-estradiol from aqueous solutions by a novel hierarchically nitrogen-doped porous carbon, J. Colloid Interf. Sci. 533 (2019) 700–708.
[55] L. Jiang, Y. Liu, S. Liu, X. Hu, G. Zeng, X. Hu, S. Liu, S. Liu, B. Huang, M. Li, Fabrication of β-cyclodextrin/poly (l -glutamic acid) supported magnetic graphene oxide and its adsorption behavior for 17β-estradiol, Chem. Eng. J. 308 (2017) 597–605.
[56] C. Ling, X. Li, Z. Zhang, F. Liu, Y. Deng, X. Zhang, A. Li, L. He, B. Xing, High Adsorption of Sulfamethoxazole by an Amine-Modified Polystyrene-Divinylbenzene Resin and Its Mechanistic Insight, Environ. Sci. Technol. 50 (18) (2016) 10015–10023.
[57] Y. Feng, G. Chen, Y. Zhang, D. Li, C. Ling, Q. Wang, G. Liu, Superhigh co-adsorption of tetracycline and copper by the ultrathin g-C3N4 modified graphene oxide hydrogels, J. Hazard. Mater. 424 (2022), 127362.
[58] J. Han, W. Qiu, Z. Cao, J. Hu, W. Gao, Adsorption of ethinylestradiol (EE2) on polyamide 612: Molecular modeling and effects of water chemistry, Water Res. 47 (2013) 2273–2284.
[59] P. Liao, Z. Zhan, J. Dai, X. Wu, W. Zhang, K. Wang, S. Yuan, Adsorption of tetracycline and chloramphenicol in aqueous solutions by bamboo charcoal: A batch and fixed-bed column study, Chem. Eng. J. 228 (2013) 496–505.
[60] M. Saood Manzar, T. Ahmad, N. Ullah, P. Velayudhaperumal Chellam, J. John, M. Zubair, R.J. Brandão, L. Meili, O. Alagha, E. Çevik, Comparative adsorption of Eriochrome Black T and Tetracycline by NaOH-modified steel dust: Kinetic and process modeling, Sep. Purif. Technol. 287 (2022) 120559.